IBRACON Structures and Materials Journal
Revista IBRACON de Estruturas e Materiais
ISSN 1983-4195 ismj.org

ORIGINAL ARTICLE

Menetrey-Willam numerical model for analysis of fiber reinforced concrete beams

Modelo numérico de Menetrey-Willam para análise de vigas de concreto armado com fibras

Lucas Meira Santos[a]
Paulo Roberto Lopes Lima[a]
Geraldo José Belmonte dos Santos[a]

[a]Universidade Estadual de Feira de Santana – UEFS, Departamento de Tecnologia, Programa de Pós-Graduação em Engenharia Civil e Ambiental, Feira de Santana, BA, Brasil

Received 01 August 2024
Revised 21 November 2024
Accepted 04 February 2025

Abstract: The introduction of fibers into cement-based materials alters, among other things, the stress-strain diagram in both tension and compression, necessitating changes in behavior models and structural design. This study evaluated the effect of stress-strain curves on the behavior of Fiber Reinforced Concrete (FRC) beams, using ANSYS software for modeling based on the finite element method (FEM). The Menetrey-Willam model, supported by the Willam-Warkne yield surface, was chosen to represent the mechanical behavior of fiber-reinforced concrete. The adopted model is capable of simulating elasticity, plasticity, tension stiffening, large displacements and deformations. To verify and validate the model, numerical simulations were conducted on FRC's behavior under compression and indirect tension (bending), and on beams subjected to 4-point tests, comparing numerical results with experimental data. The simulations demonstrated agreement with laboratory tests in tension, compression, and beam bending, affirming the feasibility of incorporating fiber effects into computer modeling, thereby modifying concrete properties. Specifically, beams subjected to flexural failure exhibited numerical responses similar to the experimental results, demonstrating the model's ability to represent the influence of fiber reinforcement on structural failure modes.

Keywords: steel fiber, reinforced concrete, Menetrey-Willam model, finite element.

Resumo: A introdução de fibras em materiais de base cimentícia altera, dentre outras coisas, o diagrama tensão-deformação, tanto na tração quanto na compressão, exigindo mudanças nos modelos de comportamento e dimensionamento estrutural. No presente trabalho, avaliou-se o efeito das curvas tensão-deformação sobre o comportamento de vigas de Concreto Armado Reforçado com Fibras (CARF), usando para a modelagem o software ANSYS, baseado no Método dos Elementos Finitos. Foi definido o modelo de Menetrey-Willam, amparado pela superfície de escoamento de Willam-Warkne, para representar o comportamento mecânico do concreto com fibras. O modelo adotado é capaz de representar o comportamento de elasticidade, plasticidade, tension stiffening e grandes deslocamentos e deformações. Para verificação e validação do modelo, foram realizadas simulações numéricas do comportamento do Concreto Reforçado com Fibras (CRF) sob compressão, tração indireta (flexão) e em vigas submetidas a ensaios de 4 pontos, comparando os resultados numéricos com dados experimentais. As soluções mostraram concordância com os ensaios laboratoriais na tração, compressão e flexão de vigas, indicando que é possível incorporar na modelagem computacional os efeitos da fibra no concreto, caracterizados pela alteração de suas propriedades. Especificamente, as vigas submetidas à ruptura por flexão tiveram respostas numéricas similares aos resultados experimentais, demonstrando a capacidade do modelo de Menetrey-Willam em representar adequadamente como o reforço de fibras influencia o modo de falha estrutural.

Palavras-chave: fibras de aço, concreto reforçado, modelo de Menetrey-Willam, elementos finitos.

How to cite: L. M. Santos, P. R. L. Lima, and G. J. B. Santos, "Menetrey-Willam numerical model for analysis of fiber reinforced concrete beams" *Rev. IBRACON Estrut. Mater.*, vol. 18, no. 2, e18211, 2025, https://doi.org/10.1590/S1983-41952025000200011.

Corresponding author: Lucas Meira Santos. E-mail: lucasufba@yahoo.com.br
Financial support: State University of Feira de Santana (FINAPESQ/034-2021) and Bahia State Research Support Foundation (BOL0305/2021).
Conflict of interest: Nothing to declare.
Data Availability: The data that support the findings of this study are available from the corresponding author, L. M. Santos, upon reasonable request.

1 INTRODUCTION

The use of fiber-reinforced concrete structures has been increasing worldwide due to the greater ductility of this material and its ability to minimize cracking in concrete under dynamic loads, such as impact and earthquakes [1]. Additionally, in structures supported on the ground, such as industrial floors, pavements, and building foundations, the use of fibers alone is sufficient to ensure mechanical strength without the need for steel mesh, which reduces both cost and production time [2]. The incorporation of fibers into the concrete enhances the material's deformation capacity by controlling the propagation of cracks resulting from external actions.

As a result of adding fibers to concrete, internal tensile stresses are transferred within the reinforced concrete element even after cracking, which modifies the structural behavior compared to concrete without fibers and allows for the maintenance of residual strength. To account for this beneficial effect of fibers, structural design codes have begun to incorporate the contribution of concrete under tension, associated with the residual stresses of fiber-reinforced concrete (FRC). However, this change remains conservative in the analysis of FRC structures because it does not consider the deformation gain that fiber-reinforced concrete achieves under compression before failure [3], [4]. Additionally, the modifications in structural behavior under shear [5], [6] and better control of localized cracks at the interface between the reinforcement and the matrix [7] confirm the contribution of fibers in improving structural behavior, which is not considered in the design codes.

More accurate models for the analysis and design of fiber-reinforced concrete have been developed using computational mechanics, employing various numerical methods in the analysis of beams [8], slabs [6], and FRC columns [9]. The main change in these analysis models, considering the presence of fibers in the concrete, is the constitutive law of the material in a fractured state, emphasizing the simulation of the structure's nonlinear behavior, as the most effective contribution of the fibers begins in the post-cracking regime. Generally, mathematical models consider the contribution of fibers through a tension-cohesion law based on semi-empirical formulations or experimental data obtained from inverse analysis [10].

One of the models used for the characterization of FRC beams is the distributed cracking model. However, these models are sensitive to the determination of the shear retention factor (β), which controls the crack opening/sliding process. High values of β cause stress locking, while low values of β lead to computational convergence problems [11]. As an alternative, parameters of mode I fracture from constitutive models for the analysis of fiber-reinforced concrete beams are obtained through inverse analysis, using experimental data from a notched three-point bending beam, as well as from tests on circular slabs. However, according to Barros et al. [10], inverse analysis can have situational applications for slabs or beams due to the different cracking processes observed in these structures, which have distinct orientations.

The Discrete Cracking Model, based on concepts of discontinuities embedded or incorporated into finite elements coupled at the interface of regular elements, has been used in the analysis of FRC structures. However, for this analysis, it is necessary to define the direction and position of the cracks before proceeding with computational modeling, presenting a limitation of structural approaches. This model is recommended only for solving problems involving push-off tests and pre-cracked structures [12].

Additionally, the analysis of FRC structures has been conducted using Damage Mechanics concepts, where the material's constitutive equations include a variable (damage) that quantifies the deterioration process [13]. A study by Pereira et al. [8] used a bilinear model to quantify the progressive losses of stiffness and strength in a post-cracking regime, based on La Borderie's homogenization rule [14]. This rule is proposed for the behavior of FRC to determine the stress correction in the damaged matrix. However, these models exhibit zones dependent on energy parameters G_f (fracture energy) and h (section height, characteristic size), which, due to the high variability of experimental responses for FRC structures, were considered insufficient for achieving good numerical convergence.

The uncertainty about the most suitable methodology for determining the parameters involved in the computational modeling of FRC was highlighted by Barros et al. [10] in a competition on the numerical simulation of steel-fiber-reinforced concrete beams failing in shear, which involved various numerical models to simulate experimental behavior. A similar study was also conducted for modeling structural elements under bending [11]. The results of both studies indicate that numerical models still need to be improved to more accurately simulate the mechanical behavior of reinforced concrete structures [11], either by refining existing models or by applying new methods.

The Menetrey-Willam (MW) numerical model, which is based on the Willam-Warnke failure surface, has increasingly been used to determine the hardening/softening rule for studying concrete [15], [16]. The model is capable of predicting the mechanical behavior of concrete subjected to complex stress states, including not only simple tension and compression states but also combinations of tension, compression, shear, and triaxial conditions that arise when the concrete is confined. Additionally, the MW model, based on plasticity theory, is less susceptible to issues of excessive strain localization (or “softening”) in finite elements, whereas distributed cracking models may require

specific regularizations to address mesh-related problems. In this sense, the MW model is more versatile and, therefore, more suitable for representing the FRC in general situations, whereas damage and distributed cracking models are more focused on capturing the progressive degradation and cracking behavior, which, macroscopically, have their effects mitigated by the presence of steel reinforcement.

According to Dmitriev et al. [17], using this model to represent the constitutive laws of plain concrete in the numerical modeling of flexural beams of Reinforced Concrete (RC) subjected to four-point bending tests resulted in good accuracy and convergence. The application of the MW model in the analysis of polymeric fiber-reinforced concrete elements without steel reinforcement was presented by Unuk and Kuhta [18], who found that computational modeling allows for the adequate definition of the residual tensile strength used in the design of fiber-reinforced concrete. In the investigation of steel fiber concrete fracture energy, Rashidi et al. [19] used the Menetrey-Willam yield surface to account for the nonlinear behavior of aggregates and cement mortar. According to the authors, numerical modeling with the Menetrey-Willam yield surface, which considers the concrete's behavior under compressive and tensile stresses, is an important tool for a broader understanding of fiber-reinforced concrete behavior.

Considering the need to improve computational methods in the modeling of reinforced concrete structures and the behavior change induced by fibers in concrete, this work aims to simulate and validate the behavior of fiber-reinforced concrete beams using the Menetrey-Willam numerical model, implemented in ANSYS Workbench 2022 R1. Initially, the MW model was calibrated with experimental results to determine the parameters that could reproduce the stress-strain behavior of fiber-reinforced concrete. Subsequently, a fiber-reinforced concrete beam was modeled, using an experimental result available in the literature, to evaluate the load-displacement behavior and cracking mode.

2 MENETREY-WILLAM MODELLING

The MW model includes parameters that can reproduce the physical nonlinearity and plasticity of materials, making it highly suitable for the numerical modeling of cement-based materials, both under tensile and compressive stress. Figure 1 illustrates the hardening and softening behavior of the yield surfaces and the mathematical functions that simulate the constitutive laws of concrete, as presented by [17].

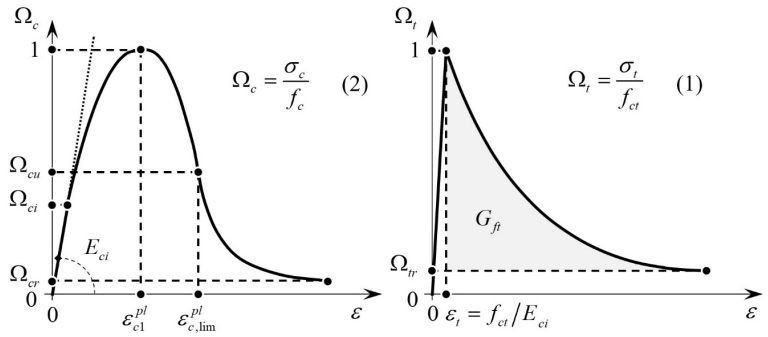

Figure 1 – Constitutive Laws - Menetrey-Willam Model: (a) Behavior under Compression and (b) Behavior under Tension [17].

The behavior under compression until reaching the peak stress, that is, during the material's hardening phase, can be described by Equation 1:

$$\Omega_c = \Omega_{ci} + (1-\Omega_{ci}) \cdot \sqrt{\frac{2 \cdot \varepsilon_c}{\varepsilon_{c1}^{pl}} - \frac{\varepsilon_c^{\,2}}{\varepsilon_{c1}^{pl\,2}}} \tag{1}$$

where Ω_c is the hardening/softening function in compression of concrete, Ω_{ci} is the stress at the onset of nonlinearity, ε_c is the strain, and ε_{c1}^{pl} is the plastic strain at peak stress. The branch corresponding to the softening of the material is divided into two segments:

For $\varepsilon_{c1}^{pl} < \varepsilon_c < \varepsilon_{c,\lim}^{pl}$:

$$\Omega_c = 1 - (1 - \Omega_{cu}) \cdot \left(\frac{\varepsilon_c - \varepsilon_{c1}^{pl}}{\varepsilon_{c,\lim}^{pl} - \varepsilon_{c1}^{pl}} \right)^2 \tag{2}$$

where $\varepsilon_{c,\lim}^{pl}$ is the plastic strain at the transition to matrix softening and Ω_{cu} corresponds to the residual stress relative to the strain at the transition point to the material's softening.

For $\varepsilon_c > \varepsilon_{c,\lim}^{pl}$:

$$\Omega_c = \Omega_{cr} + (\Omega_{cu} - \Omega_{cr}) \cdot \exp\left(2 \cdot \frac{\Omega_{cu} - 1}{\varepsilon_{c,\lim}^{pl} - \varepsilon_{c1}^{pl}} \cdot \frac{\varepsilon_c - \varepsilon_{c,\lim}^{pl}}{\Omega_{cu} - \Omega_{cr}} \right) \tag{3}$$

where Ω_{cr} is the residual relative stress of the compressed concrete.

For concrete under tension, the model uses the generalized Hooke's law until reaching the maximum stress f_{ct}. After reaching this limit, the softening function is based on an exponential equation that gradually reduces the tensile strength, as expressed in Equation 4:

$$\Omega_t = \exp\left(-\frac{\varepsilon_t}{a_t} \right) \tag{4}$$

where ε_t and Ω_t correspond to the strain and relative stress of the concrete under tension, respectively, while a_t is a coefficient determined by:

$$a_t = \frac{g_{ft}}{f_{ct}} \quad ; \quad g_{ft} = máx\left\{ \frac{G_{ft}}{L_i}, \frac{f_{ct}^{\,2}}{E_{ci}} \right. \tag{5}$$

where G_{ft} is the fracture energy of the concrete under direct tension, L_i is the effective length of the element, f_{ct} is the characteristic tensile strength of the concrete, and E_{ci} is the initial modulus of elasticity of the concrete. The relationship for the energy dissipated during the material's softening follows Equation 6. This equation represents the yield function of the concrete under tension.

$$\int_0^\infty \Omega_t \cdot d\varepsilon = \frac{g_{ft}}{f_{ct}} \tag{6}$$

The softening limit of the material is defined by Ω_{tr} [17], as indicated in Figure 1.

3 METHODOLOGY

3.1 Numerical modeling

3.1.1 Representation of materials

For the representation of concrete, the CPT215 element was used (Figure 2a), which replicates the effects of elasticity, plasticity, stress stiffening, large deflections, and deformations. It is a three-dimensional linear element composed of 8 nodes, with 3 degrees of freedom at each node. Its characteristics are suitable for modeling cementitious materials due to its physical and mechanical configuration, and particularly its ability to transmit stresses in a post-cracking regime.

In the case of fiber-reinforced concrete, the composite was indirectly modeled by altering the constitutive laws of the material, considering it as a single homogenized entity with these laws compatible with the MW numerical model, based on plasticity theory.

The reinforcement was modeled using the REINF264 element (Figure 2b), which represents linear bodies with 2 nodes and 3 degrees of freedom at each node. The numerical modeling of the steel bars was characterized by a perfect elastoplastic material, defined by a bilinear stress-strain curve implemented through the mechanical properties of the material.

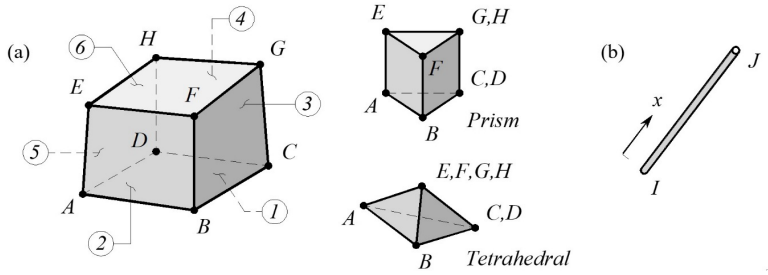

Figure 2 – Finite elements used for (a) concrete (CPT215) and (b) steel (REINF264)

3.1.2 Parametric Study

To evaluate the effect of each parameter of the MW model on the stress-strain behavior of the material, a numerical simulation was conducted applying both positive and negative displacements to the top face of a concrete cube with a 150 mm edge length (Figure 3). Considering the symmetry, one-eighth of the cube was modeled using symmetry faces as boundary conditions, with CPT215 finite elements of 5 mm side length.

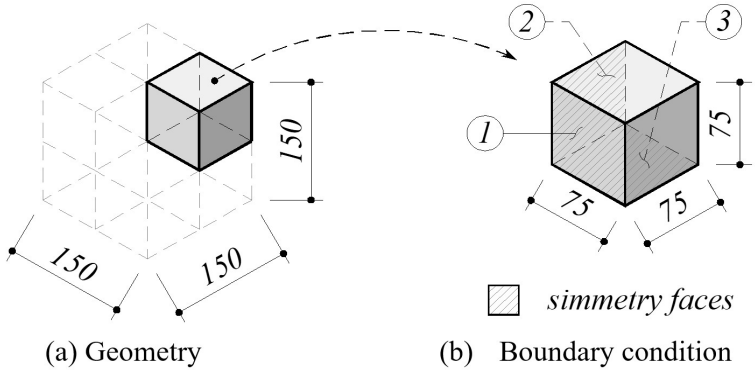

Figure 3 – Structure idealized for the parametric study of the MW model

Table 1 shows the mechanical properties of the concrete with material data used by Dmitriev et al. [17] for the investigation of the Menetrey-Willam model parameters.

Table 1 – Material Mechanical Properties

Symbol	Parameter Name	Unit	Value
E_{ci}	Tangent Modulus of Elasticity	GPa	36.5
υ	Poisson's Ratio	-	0.20
f_c	Uniaxial Compressive Strength of Concrete	MPa	40
f_{ct}	Uniaxial Tensile Strength of Concrete	MPa	3.5
f_{bc}	Biaxial Compressive Strength of Concrete	MPa	46.4

Source: Dimitriev (2020)

The following parameters were evaluated: plastic deformations ε_{c1}^{pl} (ranging from 0.1 to 1.9 $\cdot 10^{-3}$ mm/mm) and $\varepsilon_{c,\lim}^{pl}$ (ranging from 2 to 6 $\cdot 10^{-3}$ mm/mm), relative stresses Ω_{ci} (ranging from 0.1 to 0.7), Ω_{cu} (ranging from 0.3 to 1.0), Ω_{cr} and Ω_{tr} (both ranging from 0.05 to 0.15), as well as the specific fracture energy G_{ft} (ranging from 5.0 to 10.0 N/m).

3.1.3 Calibration of the Model for Fiber-Reinforced Concrete under Compression

In this study, a numerical analysis of compressed concrete was conducted, referencing the experimental study by Barros [6]. The model geometry was idealized as a cylinder with a diameter of 150 mm and a height of 300 mm, corresponding to the dimensions of the uniaxial compression test. Boundary conditions were set similarly to those used in the parametric study. A convergence study of the model was conducted with the objective of analyzing the efficiency of the mesh discretization. Initially, the element with a size of 50 mm was simulated. Following this, mesh refinement was performed using smaller element sizes of 25, 10, and 7.5 mm. A stress-strain curve was generated, where the curves produced were analyzed considering the variations in the element dimensions. The minimum tolerance for the highest stress to validate the convergence study was set at 10^{-3}, aiming to ensure greater reliability in the quality of the finite element discretization. In this case, the 7.5 mm element was chosen, as it met the minimum tolerance (Figure 4).

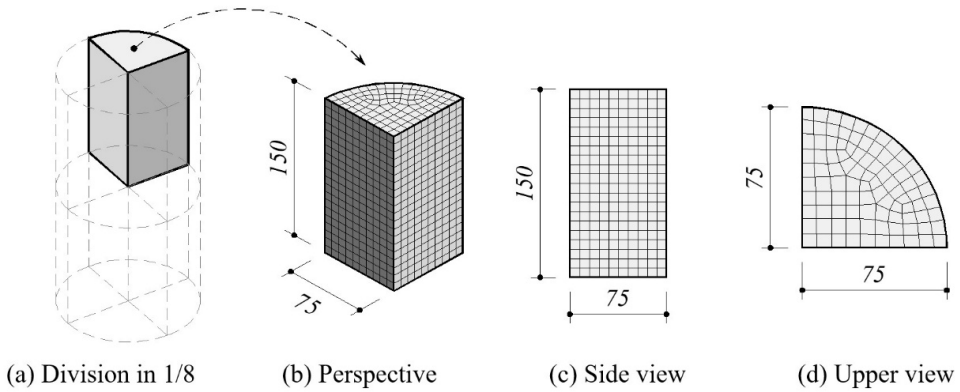

Figure 4 – Model using FEM for concrete subjected to compression (dimensions in mm)

As the loading condition, an incremental displacement of 1.0 mm downward was applied to the top face of the structure. The fiber content ranged from 0 to 60 kg/m^3. Table 2 presents the data available from the author's experimental study:

Table 2 – Experimental Results from Barros for PC and FRC under Compression

MAT	ε_{c1}	$\varepsilon_{c,\lim}$	E_{ci}	S_d [1]	$\sigma_{c,\lim}$
	[mm/mm]	[mm/mm]	[MPa]	[MPa]	[MPa]
CS	0.0026	0.0050	20.622	622	1.5
FRC30	0.0026	0.0064	19.498	1.756	3.5
FRC45	0.0028	0.0084	19.831	1.072	4.9
FRC60	0.0033	0.0114	18.722	1.888	4.2

Source: Adapted from Barros [6]

[1] Standard deviation of the initial modulus of elasticity

The calculation of the parameters involved in the MW model is essential for defining the constitutive laws of the model. The value of the relative stress Ω_{ci} is approximately 40% of the characteristic compressive strength of the concrete [20]. However, in the absence of experimental data, Equation 7 can be used to calculate this parameter:

$$\Omega_{ci} = \frac{f_c^{1.855}}{60 \cdot f_c} \tag{7}$$

Where f_c is the concrete's ultimate compressive stress. The constants Ω_{cu}, ε_{c1}^{pl} and $\varepsilon_{c,\lim}^{pl}$ can be determined from laboratory results, with Ω_{cu} typically around 50% of the peak strength. For the residual stress Ω_{cr}, a value between 0.05 and 0.15 can be assumed for plain concrete [20], with this range also applicable to fiber-reinforced concrete [6]. According to plasticity theory, the total strain ε_c^{to} can be represented as the sum of elastic and plastic strains:

$$\varepsilon_c^{to} = \varepsilon_c^{el} + \varepsilon_c^{pl} \tag{8}$$

Where ε_c^{el} is the elastic strain and ε_c^{pl} is the plastic strain. Thus, the plastic strain corresponding to the peak stress ε_{c1}^{pl} can be calculated as:

$$\varepsilon_{c1}^{pl} = \varepsilon_{c1} - \varepsilon_c^{el} \quad \rightarrow \quad \varepsilon_{c1}^{pl} = \varepsilon_{c1} - \frac{f_c}{E_{ci}} \tag{9}$$

According to Dmitriev et al. [17], for plain concrete, the total strain corresponding to the peak stress ε_{c1} can be defined as the lesser of two values determined as follows:

$$\varepsilon_{c1} = mín \begin{cases} -0.0022 \\ -\dfrac{0.7 \cdot f_c^{\,0.31}}{1000} \end{cases} \tag{10}$$

The plastic strain at the point of matrix softening $\varepsilon_{c,\lim}^{pl}$, also known as the limiting plastic strain, is defined by Equation 11:

$$\varepsilon_{c,\lim}^{pl} = \varepsilon_{c,\lim}^{to} - \frac{f_{c,\lim}}{E_{ci}} \tag{11}$$

Where $\varepsilon_{c,\lim}^{to}$ ranges from 2.4 to 4.2‰ for concretes with strengths up to 80 MPa [20].

The biaxial compressive strength of concrete is obtained empirically using Equation 12 from the CEB-FIP code [20]:

$$f_{bc} = \left(1.2 + \frac{f_c}{1000}\right) \cdot f_c \tag{12}$$

To determine the peak tensile strength of concrete, Equations 13 and 14 from NBR 6118 [21] are used.

For concrete with grades up to C50, the following applies:

$$f_{ct} = 0.3 \cdot f_c^{\,2/3} \tag{13}$$

For concrete with grades C55 to C90, the following applies:

$$f_{ct} = 2.12 \cdot \ln\left(1 + 0.11 \cdot f_c\right) \tag{14}$$

A summary of the parameters used in Barros's numerical modeling is presented in **Table 3**:

Table 3 – Final parameters for Barros's numerical modeling, used in the numerical analysis of compression and indirect tension: E_{ci} (Gpa); f_c (MPa); f_{ct} (MPa); f_{bc} (MPa); ψ (º); ε_{c1}^{pl} (10^{-3} mm/mm); $\varepsilon_{c,\lim}^{pl}$ (10^{-3} mm/mm); G_{ft}^{R} (N/m).

MAT	E_{ci}	υ	f_c	f_{ct}	f_{bc}	ψ	ε_{c1}^{pl}	$\varepsilon_{c,\lim}^{pl}$	Ω_{ci}	Ω_{cu}	Ω_{cr}	G_{ft}^{R}	Ω_{tr}
PC	21.244	0.20	36.3	3.29	42.2	9	0.79	4.18	0.359	0.478	0.041	34.53	0.15
FRC30	21.254	0.20	35.7	3.25	41.6	9	0.92	5.51	0.354	0.530	0.098	297.13	0.15
FRC45	20.903	0.20	36.4	3.30	42.4	9	1.06	5.90	0.360	0.575	0.135	408.25	0.15
FRC60	20.610	0.20	34.0	3.15	39.6	9	1.65	9.01	0.340	0.600	0.124	462.83	0.15

Source: The author

3.1.4 Model Calibration for Fiber-Reinforced Concrete under Indirect Tension

The geometry of the analyzed structure is represented by a notched beam produced by Barros [6], who conducted experimental studies considering both plain and fiber-reinforced concrete, as well as simulated computationally the notched beam using a distributed cracking model. Following the same criteria as the numerical analysis under compression, symmetry planes were used to model one-quarter of the beam. The finite element mesh refinement was achieved with elements measuring 7.5 mm. A 2 mm downward displacement was applied at the central and upper points of the beam. The proposed static system for the modeling is shown in Figure 5.

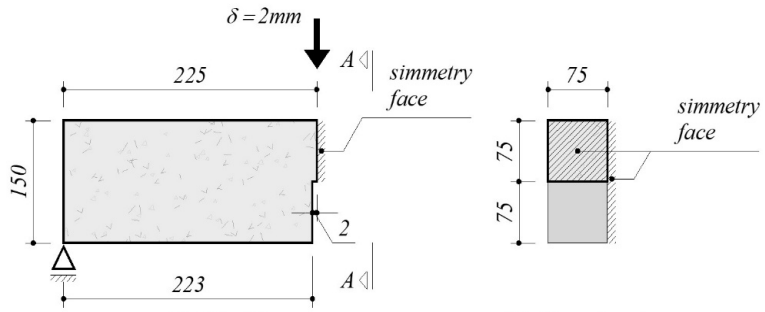

Figure 5 – Idealized Model for Notched Beam

After completing the numerical solution, the residual stress f_{fnet} was calculated based on Equation 15, as proposed by Barros [6]:

$$f_{fnet} = 1.5 \cdot \frac{\left[F + 0.5 \cdot m_1 \cdot g \cdot \left(1 - \alpha^2\right) + m_2 \cdot g\right]}{b \cdot \left(d - a\right)^2} \cdot l \tag{15}$$

where F is the force transmitted by the equipment, m_1 is the mass of the test specimen between supports, m_2 is the mass of the equipment that monitors the deformation during the test, L is the total length of the specimen, l is the length between supports, g is the acceleration due to gravity, b is the width of the specimen, and a is the height of the notch, with $\alpha = L/(l-1)$.

The dilatancy angle ψ of the concrete, a property that characterizes the nonlinear volume increase associated with shear distortion, ranges from 8 to 15º [22]. In this study, a value of 9º was chosen based on the numerical study by Dmitriev et al. [17]. The relative stress of the tensile concrete Ω_{tr} was defined as 5% of the peak stress [17]. The MW model defines the fracture energy through uniaxial tensile testing, associated with Mode I fracture (opening by tension). In the absence of experimental data, the formula for determining this parameter for plain concrete, is described by Equation 16:

$$G_{ft} = G_{ft0} \cdot \left(\frac{f_c + 8}{10}\right)^{0.7} \tag{16}$$

where G_{ft0} is defined with respect to the $d_{máx}$ of the aggregate. On the other hand, experimental data can be used to approximately determine the direct tensile fracture energy G_{ft} of the matrix from the area under the curve of the constitutive law of the tensile concrete (Figure 6).

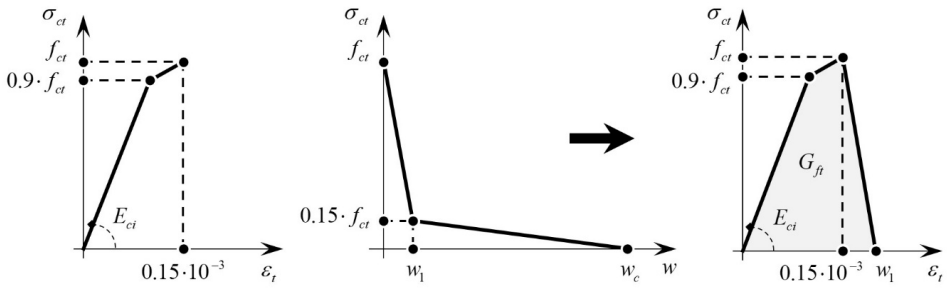

Figure 6 – Constitutive Law of Tensile Concrete (Adapted from CEB-FIP [20])

Pereira [23] conducted direct tensile tests, obtaining results for strength and deformations of concrete reinforced with up to 157 kg/m³ of steel fibers. Thus, the calculation of the approximate fracture energy G_{ft}^{R} for the composite follows the Equation 17:

$$G_{ft}^{R} = 0.5 \cdot \varepsilon_{G_{ft}^{R}} \cdot L_i \cdot f_{ct}^{R} \tag{17}$$

where $\varepsilon_{G_{ft}^{R}}$ is the peak strain, L_i is the effective length of the specimen, and f_{ct}^{R} is the tensile strength of the fiber-reinforced concrete. The final summary of the parameters used in Barros' numerical modeling is provided in Table 3.

3.1.5 Numerical Modeling of Beams under Flexure

The validation of the numerical modeling of the beams considered experiments conducted by Pajak and Wandzik [24]. The study focused on the use of recycled steel fibers (originating from tires) embedded in the matrix, enhancing the load-carrying capacity of reinforced concrete beams. The work focused on beams under four-point bending, incorporating a fiber content of 40 kg/m³. The structural arrangement was used to analyze the contribution of the fibers to the load-carrying capacity of the beams, cutting the upper longitudinal reinforcements to avoid considering the effect of double reinforcement. The stirrups in the support region were designed to increase shear resistance and guide failure to occur by bending. The geometry and arrangement of the beam reinforcements are shown in Figure 7.

A perfect bond was assumed at the interface between the reinforcements and the concrete. For failure, an incremental displacement of 22 mm downward was applied at the load application point. A convergence study was performed, achieving a finite element size of 10 mm, validating the minimum tolerance of 10^{-3} for the maximum displacement $\delta_{máx}$. The calculation of concrete shortening in the upper region of the section was approximated using the relationship between the variation in displacement ΔL (obtained numerically) and the effective length $L_i = 250\,mm$. This assumption is valid for small deflections in beams, as the variation between horizontal strain and actual strain (considering curvature) is very small. The computational representation of the total equivalent deformations of the concrete was interpreted, similarly, as a mapping of the cracks to which the element is subjected [25]. Thus, the idealized model for the numerical analysis of the beams is illustrated in Figure 8.

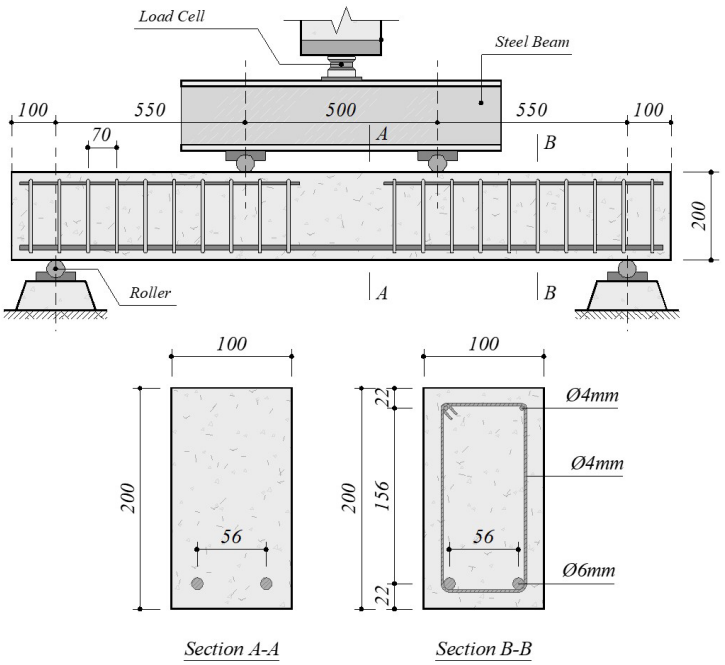

Figure 7 – Geometry and Detailing of the Beam (dimensions in mm) (Adapted from Pajak and Wandzik [24])

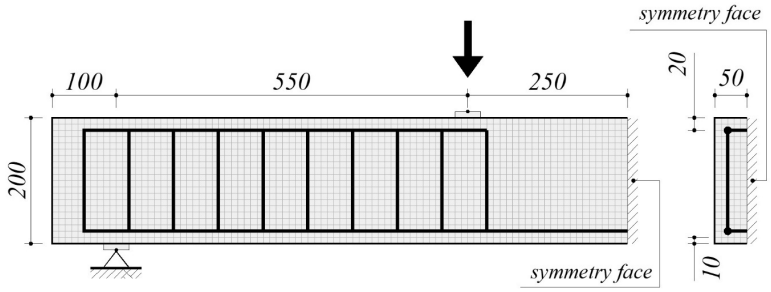

Figure 8 – Idealized Numerical Model of the Beams by Pajak and Wandzik [24] (dimensions in mm)

4 RESULTS AND DISCUSSIONS

4.1 Modeling of Fiber-Reinforced Concrete under Compression

4.1.1 Analysis of Menetrey-Willam Parameters

The configuration of the stress-strain curve for concrete, according to the MW model, is governed by four model parameters related to plastic deformation and residual stress, as shown in Figure 9.

The strain associated with the peak stress is one of the most important parameters in the stress-strain curve, as it indicates the strain corresponding to the highest stress endured by the material and the curve's inflection point. In the MW model, this property is associated with the parameter ε_{c1}^{pl}, which is assigned to the plastic strain at this peak stress. Increasing this parameter alters the numerical curve by shifting the peak to the right, as can be observed in Figure 9a. Considering the effect of fiber addition on strain and peak stress [6], this parameter, which can be indirectly correlated to fiber reinforcement, shows significant sensitivity in the material behavior. A study by Lima et al. [26] demonstrates that the introduction of fibers into concrete can result in a variation of up to 30% in the peak strain, validating a particular characteristic of fiber-reinforced concrete after the formation of the first cracks, where fibers play a crucial role in stress transfer.

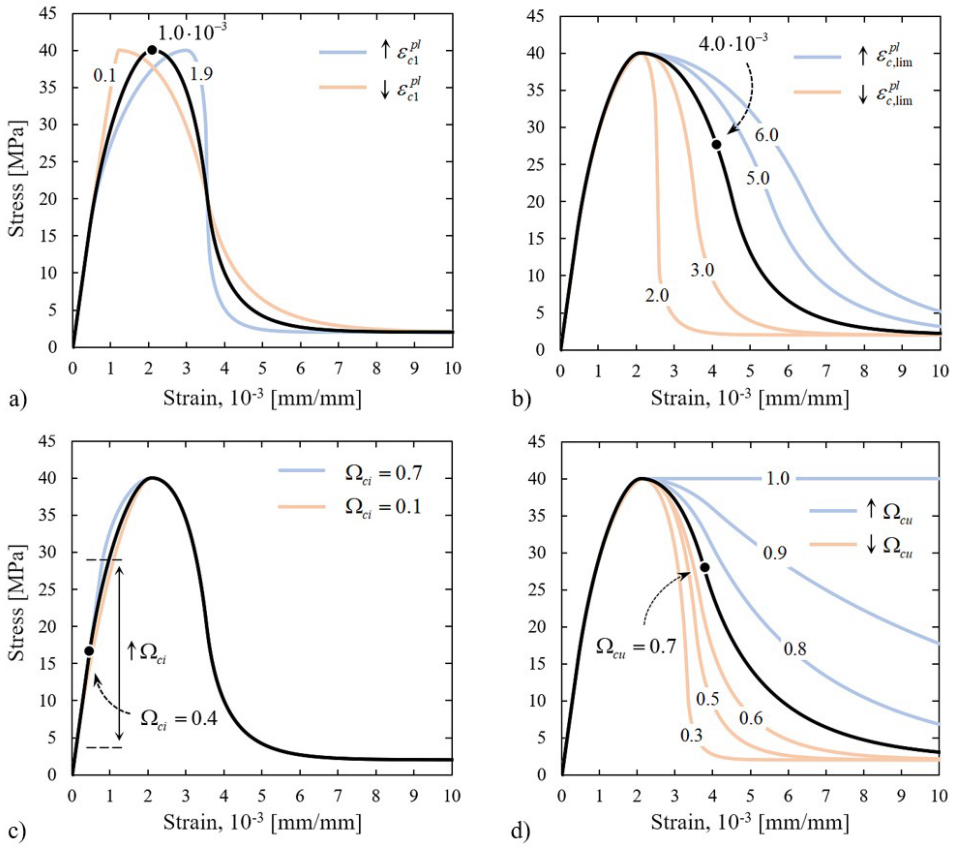

Figure 9 – Effect of Model Parameters on the Stress-Strain Curve: Parametric Study of Deformation: a) Plastic Deformation ε_{c1}^{pl} ; b) Plastic Deformation $\varepsilon_{c,\lim}^{pl}$; c) Relative Residual Stress Ω_{ci} , and d) Relative Residual Stress Ω_{cu} :

The variation of the $\varepsilon_{c,\lim}^{pl}$, parameter corresponding to plastic strain, can be associated with the toughness of concrete under compression, as it represents the strain where the curvature transition occurs in the post-cracking branch. An increase in this transition causes a rightward shift of the curve, raising the material's ultimate strain, as observed in Figure 9b. The addition of fibers to concrete reduces crack propagation and improves structural ductility after the peak load by controlling microcracks and redistributing stresses. This enhances the material's toughness, allowing for greater energy absorption and a more uniform distribution of stresses in the post-peak regime [26]. Thus, determining the $\varepsilon_{c,\lim}^{pl}$ parameter is crucial for correlating the MW model with experimental results, serving as a relevant factor for the calibration and validation of models with experimental studies.

The relative stress at the onset of physical nonlinearity Ω_{ci} represents the threshold for behavior governed by the generalized Hooke's law. This establishes a portion of the uniaxial compressive strength of concrete at which nonlinear behavior begins. When the value of Ω_{ci} is altered, the line defining this limit changes, always depending on the value adopted for the peak compressive strength of the concrete. Figure 9c shows the changes in the curvature when the value of Ω_{ci} is modified. It is observed that for the accepted peak stress value of 40 MPa, the behavior of $\Omega_{ci} = 0.70$ develops linearly up to a stress of 28 MPa. On the other hand, the curve defined by nonlinearity begins at 4 MPa when a value of $\Omega_{ci} = 0.10$ is established.

The Ω_{cu} parameter is associated with the stress at which the transition occurs in the post-peak segment of the stress-strain curve. A variation of this parameter between 0.3 and 1.0, as shown in Figure 9d, indicates that it is possible

to reproduce simple concrete without fibers or concrete with varying fiber contents, where the post-cracking behavior approaches that of an elastoplastic material (Ω_{cu} = 1). The CEB-FIP (1990) indicates material softening after reaching the peak stress, where the Ω_{cu} value is around 50% of the compressive strength. The NBR 6118 (2023) considers perfect elastoplastic behavior for concrete under compression. Analyzing the parametric study, increasing the Ω_{cu} parameter reduces the strength drop up to the ultimate strain of the material, thereby achieving similarity with the constitutive law defined by the Brazilian standard (Figure 10).

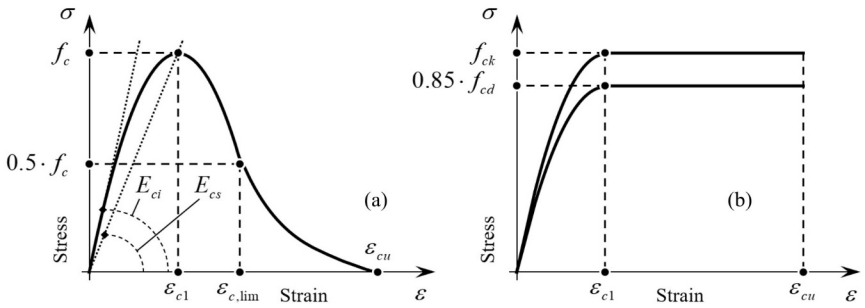

Figure 10 – Theoretical Curves, Stress-Strain for Compressed Concrete: (a) Curve according to (CEB-FIP, 1990), (b) Curve according to (NBR 6118, 2023)

The Ω_{cr} parameter exhibits a direct relationship with the residual stress of concrete. By increasing the value of this parameter, a curve with higher resistance to residual deformations can be obtained. Figure 11 shows the changes in the curvature when the Ω_{cr} value is increased.

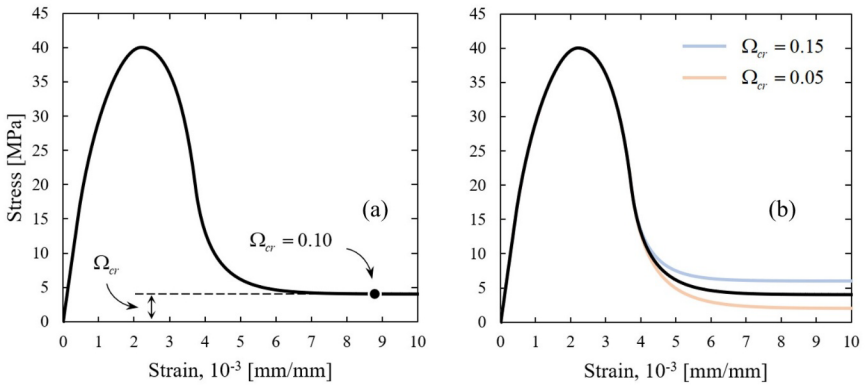

Figure 11 – Parametric Study of the Relative Residual Stress Ω_{cr} : (a) Reference Point Ω_{cr} , (b) Variation of Ω_{cr} in the Curve

4.1.2 Validation of the Numerical Model

The numerical modeling, performed using the MW model, produced satisfactory results for plain and fiber-reinforced concrete. Figure 12 presents the numerical results of the present work, comparing them with the experimental results obtained by Barros [6].

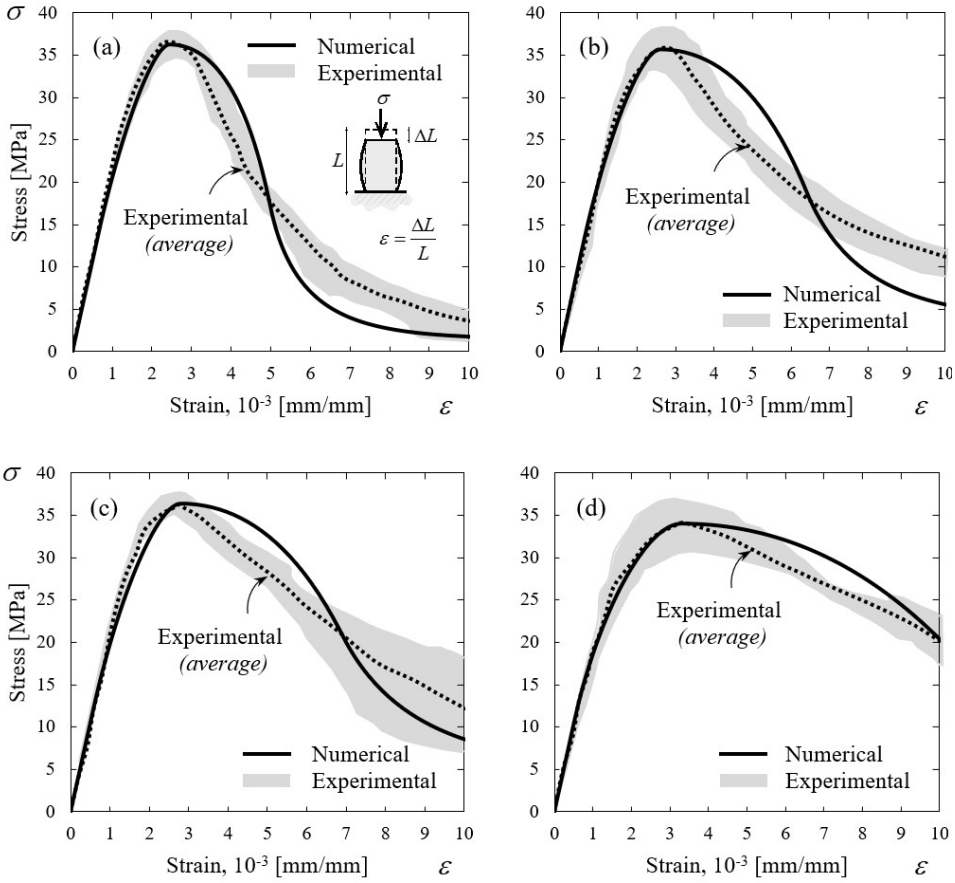

Figure 12 – Numerical and Experimental Results of Barros [6] in Compression: (a) Concrete without fibers, (b) Concrete with 30 kg/m^3 of fibers, (c) Concrete with 45 kg/m^3 of fibers, and (d) Concrete with 60 kg/m^3 of fibers.

With the convergence of results, a correlation was made between the numerical model parameters and the fiber content. According to the parametric study, ε_{c1}^{pl} and Ω_{cu} show significant sensitivity to the mathematical functions of the material's constitutive law under compression and are also important elements for design. Thus, a relationship was established that weights the model parameters by multiplying a factor corresponding to the fiber content in the matrix. The following equations are defined as:

$$\overline{\varepsilon_{c1}^{pl}} = X \cdot \varepsilon_{c1}^{pl} \quad \rightarrow \quad X = \overline{\varepsilon_{c1}^{pl}} \,/\, \varepsilon_{c1}^{pl} \tag{18}$$

$$\overline{\Omega_{cu}} = W \cdot \Omega_{cu} \quad \rightarrow \quad W = \overline{\Omega_{cu}} \,/\, \Omega_{cu} \tag{19}$$

Where $\overline{\varepsilon_{c1}^{pl}}$ is the plastic strain at the peak stress for fiber-reinforced concrete, X is the dimensionless factor representing the fibers in the matrix for ε_{c1}^{pl}, $\overline{\Omega_{cu}}$ is the relative stress at the transition point to softening for fiber-reinforced concrete, and W is the dimensionless factor representing the fibers in the matrix for Ω_{cu}. Figure 13 shows graphs indicating the correlation between fiber content and the parameters of the numerical model.

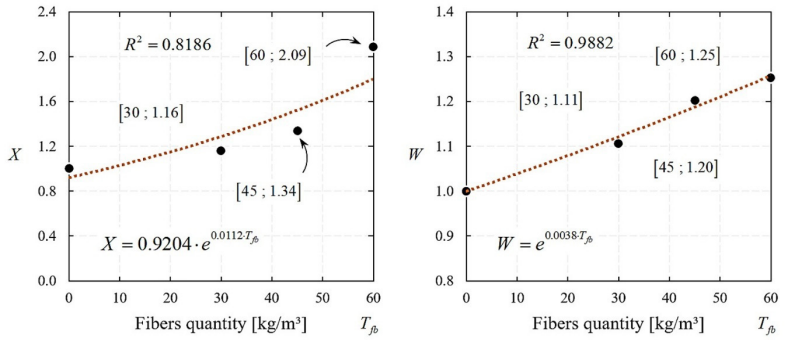

Figure 13 – Correlation between Fiber Content and ε_{c1}^{pl} and Ω_{cu}: (a) Correlation between T_{fb} and ε_{c1}^{pl}; (b) Correlation between T_{fb} and Ω_{cu}.

4.2 Modeling the Behavior of Fiber-Reinforced Concrete under Tension

4.2.1 Analysis of Menetrey-Willam Parameters

The stress-strain behavior of fiber-reinforced concrete cubes under direct tension is presented in Figure 14a. In the numerical model, one of the parameters that significantly influences the mechanical behavior is the fracture energy G_{ft}, which is sensitive to strain rates that alter the material's behavior under tension [27]. Figure 14b shows that the post-cracking behavior of the stress-strain curve varies according to the value of G_{ft}, which ranged from 5 to 10 N/m.

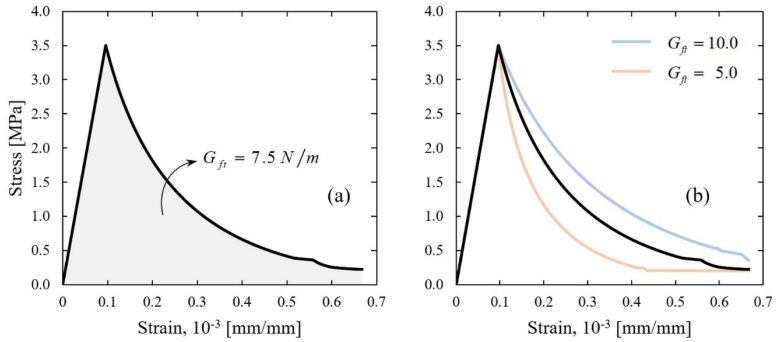

Figure 14 – Parametric Study of Fracture Energy G_{ft}: (a) Reference Area G_{ft}, (b) Variation of G_{ft} in the Curve

When dealing with residual stress, it is crucial to consider this resistance limit. Thus, the Ω_{tr} parameter is responsible for defining this resistance limit for the fracture zone of tensioned concrete. Figure 15 shows how the residual stress changes as Ω_{tr} is increased .

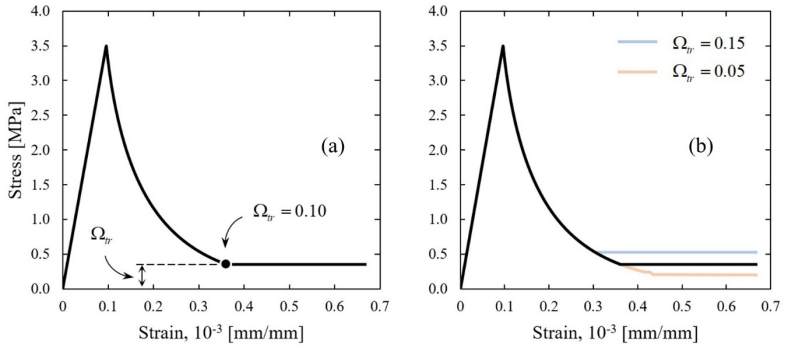

Figure 15 – Parametric Study of Relative Residual Stress Ω_{tr}: (a) Reference Point Ω_{tr}, (b) Variation of Ω_{tr} in the Curve

4.2.2 Numerical Analysis of FRC in Indirect Tension

The numerical simulation of the notched beams tested by Barros [6] demonstrated satisfactory behavior and a good representation of the fracture energy calculated for plain concrete and fiber-reinforced concrete with up to 45 kg/m^3 of fiber content. For higher amounts, such as 60 kg/m^3, the MW model does not accurately represent the behavior, both experimental and numerical [6], of the material under indirect tension (bending), as seen in Figure 16d. This is because, when a high fibers content is introduced as reinforcement, the numerical function of the MW model that defines the matrix softening does not correspond to the hardening effect after the peak stress in tension is reached.

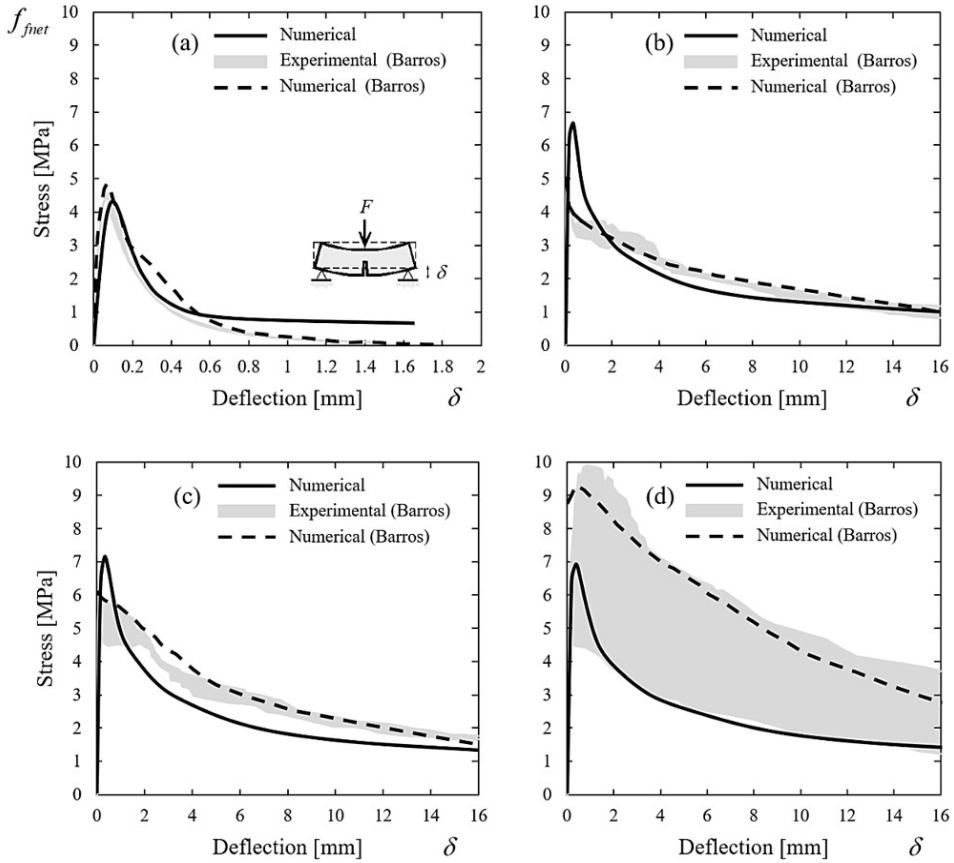

Figure 16 – Numerical and Experimental Results of Barros [6] in Indirect Tension: (a) Concrete without fibers, (b) Concrete with 30 kg/m^3 of fibers, (c) Concrete with 45 kg/m^3 of fibers, and (d) Concrete with 60 kg/m^3 of fibers.

The numerical curves from the MW model and the distributed cracking models developed by Barros [6] begin to diverge more significantly as the fiber content increases. In the numerical model used by Barros, fracture modes I and II are simulated in the constitutive laws assigned to the cracks, enhancing energy capacity in mode I and increasing shear resistance, as indicated in mode II. Thus, a certain limitation in the MW model for higher fiber contents can be identified, which, consequently, contributes to shear retention in the post-cracking regime. After the result convergence, Figure 17 shows a developed graph that correlates the portion corresponding to fiber reinforcement, following Equation 20. Equation 21 represents the trend line for determining the fiber reinforcement portion for contents ranging from 0 to 160 kg/m^3.

$$\Delta G_{ft,fb} = \frac{G_{ft}^{R}}{G_{ft}} \tag{20}$$

$$\Delta G_{ft,fb} = 0.1616 \cdot T_{fb} + 1 \tag{21}$$

Where G_{ft} and G_{ft}^{R} are the fracture energies of plain and fiber-reinforced concrete under direct tension, respectively, and $\Delta G_{ft,fib}$ is the dimensionless factor accounting only for the effect of the fibers.

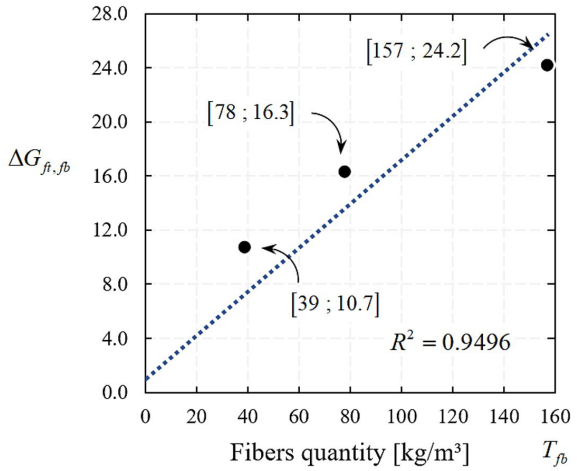

Figure 17 – Correlation between Fiber Content and Fracture Energy

4.3 Numerical Analysis of Fiber-Reinforced Concrete Beams

The numerical modeling of the beams by Pajak and Wandzik [24] produced coherent responses, being validated for both reinforced concrete and fiber-reinforced concrete. The numerical simulation accurately reproduced the stiffness loss caused by the cracking phase, as well as the onset of plastic behavior of the flexural reinforcement. The modeling of fiber-reinforced concrete beams resulted in greater stiffness before the steel plastic deformation, compared to the experimental response. This discrepancy can be justified by the fact that the numerical model does not account for microstructural damage at the interface between the reinforcement and the concrete, which, in reality, causes stiffness loss in the element during the fractured state. Figure 18 shows comparative load-displacement graphs between the numerical and experimental results.

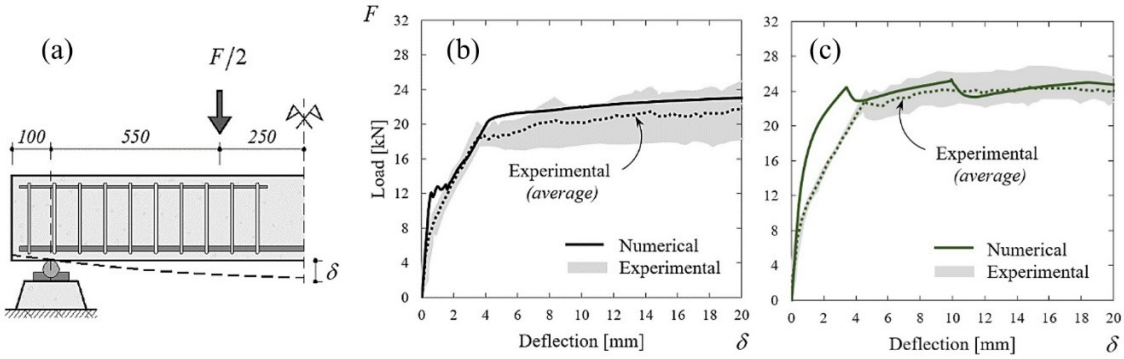

Figure 18 – Numerical and Experimental Results of Pajak and Wandzik [24] in Bending: (a) Static Scheme of the Beam (dimensions in mm), (b) Reinforced Concrete without Fibers, (c) Reinforced Concrete with 40 kg/m^3 of Fibers

The modeling results showed that the reinforced concrete beams, at failure, did not reach failure in the concrete, exhibiting a deformation of 1.3‰ (Figure 19a) in the top fiber and compression stresses of 22.9 MPa (Figure 20a), which are lower than the limits established by the materials. Additionally, the beam showed high-intensity cracks on the tensioned face (Figure 21a), which led to the rupture of the steel, as can be seen in Figure 22a. The beam simulated with fibers exhibited a higher load-carrying capacity before the steel plasticization, resulting in increased structural resistance, reaching a value of 24 kN compared to 21 kN for the beam without fibers (Figure 18).

Numerically, increasing the parameters of the MW model, specifically the fracture energy, enhances the load-carrying capacity in both compression and tension, as the stress drop does not occur as abruptly. This results in an increased bending resistance of fiber-reinforced concrete beams because, after reaching the concrete's resistance limits, the finite element of the material starts to deform while maintaining stresses due to the altered toughness from the

modification of the stress-strain curve by the fibers. Thus, there is a better stress distribution (Figure 20b) and control of deformations, displaying “cracks” in bending with less vertical propagation, albeit more numerous but of lower intensity (Figure 21b), validating the actual effect characteristic of fiber-reinforced concrete beam behavior, also observed in Pajak and Wandzik’s experiments [24] (Figure 23).

Physically, when the matrix reaches tensile strength, the fibers better control the cracks through their anchoring assistance, limiting their progression in the section. Consequently, the restriction of crack opening due to pull-out effects minimizes vertical crack propagation, ensuring greater stiffness. Additionally, the inclusion of fibers in the concrete allows the matrix to absorb more energy, as already observed in tension, and even in compression, additional shear resistance is noted after material rupture, thus increasing the beam's load-carrying capacity.

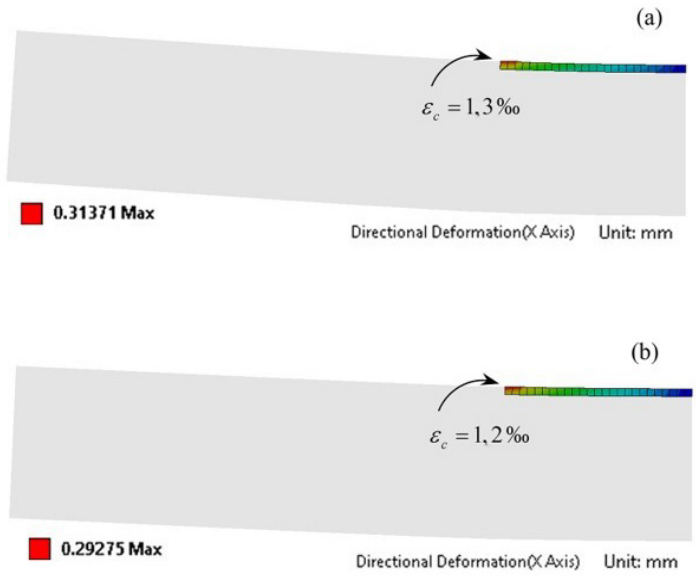

Figure 19 – Strain in Concrete at Failure: (a) RC, (b) FRC

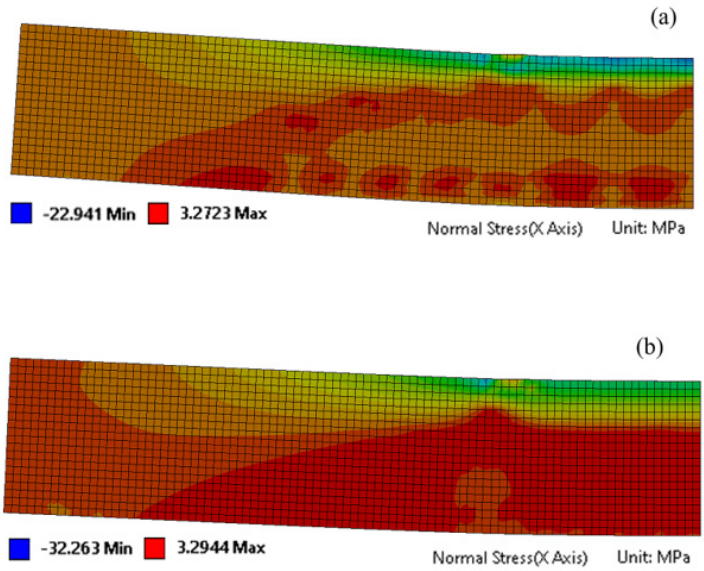

Figure 20 – Stress in Concrete at Failure: (a) RC, (b) FRC

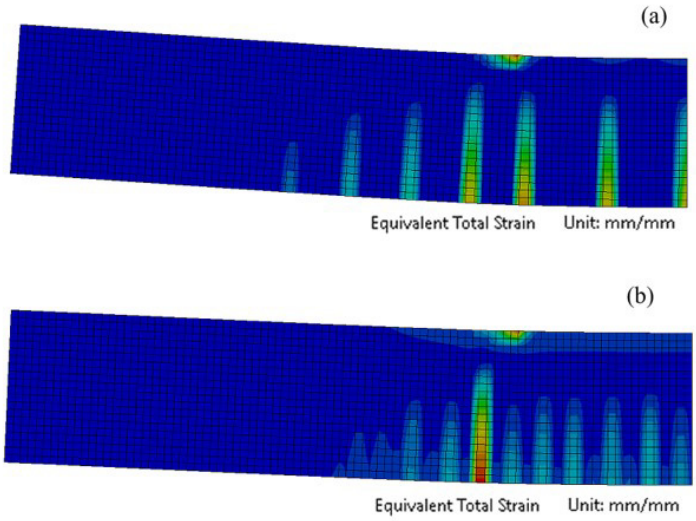

Figure 21 – Cracking in Concrete at Failure: (a) RC, (b) FRC

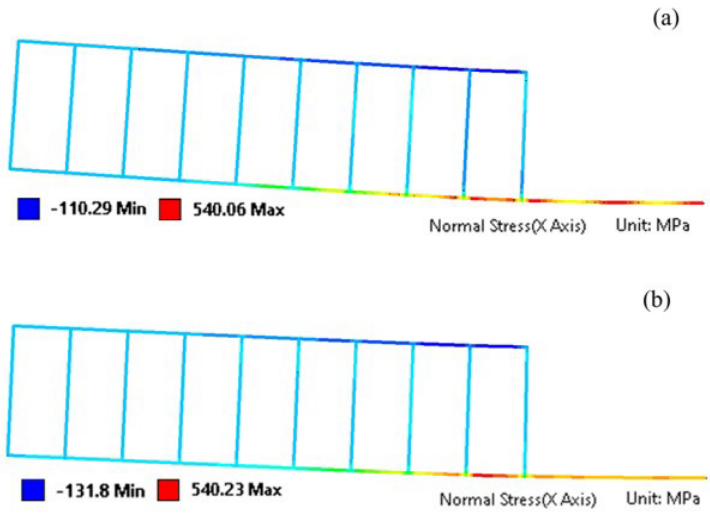

Figure 22 – Uniaxial Stress in Steel at Failure: (a) RC, (b) FRC

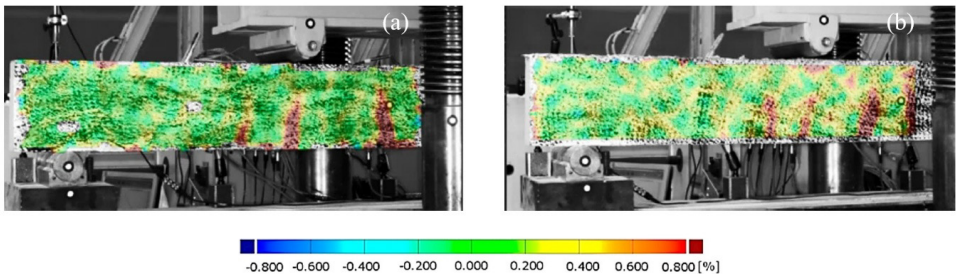

Figure 23 – Distribution of Principal Strains on the Concrete Surface, Observed in Pajak and Wandzik's Experimental Test [24]: (a) RC, (b) FRC

5 CONCLUSIONS

The MW model, in general, provided results consistent with experimental data, demonstrating that it is possible to simulate, via FEM, the effects of fibers in the matrix based on flow plasticity theory. In uniaxial compression, the numerical results were coherent, validating the model for fiber matrices with strengths lower than 40 MPa and fiber contents up to 60 kg/m^3. However, for indirect tension (bending), the mathematical functions were consistent in characterizing the FRC up to 45 kg/m^3 of fiber content. They did not, however, account for the hardening effect present in composites reinforced with higher fiber contents (e.g., 60 kg/m^3). This revealed a limitation of the numerical model used for the computational simulation of the material when there is a gain in mechanical strength in tension, even after reaching the ultimate stress.

The changes in the stress-strain curve of concrete, both in compression and tension, aimed at numerically representing the action of fibers in the matrix, resulting in good convergence when compared with experimental data from four-point flexural tests on fiber-reinforced concrete beams. The increase in stiffness and better stress distribution in the beam indicated that the model behavior was equivalent to that observed in the beams tested by Pajak and Wandzik [24], demonstrating valid numerical responses. This shows that the numerical model could capture the toughness effect imposed by the steel fibers.

It can be concluded that the MW model, by adjusting the data defining the stress-strain curve of fiber-reinforced concrete through the plasticity model, is suitable and presents a viable and highly potential option for numerical analysis of fiber-reinforced concrete beams, as its parameters can be adjusted in conjunction with the fiber content.

As a suggestion for further research, it is proposed to study the microstructural damage in the contact region between reinforcement and the fiber matrix, caused by stiffness loss in the post-cracking regime. The objective is to analyze the contribution of fibers to the adhesion of deformed bars. Refining this aspect may lead to a better diagnosis of numerical results, providing a more realistic mechanical behavior of fiber-reinforced concrete beams.

ACKNOWLEDGMENTS

The authors would like to thank FAPESB (Bahia State Research Support Foundation) for granting the master's scholarship to the first author (Scholarship Grant Term Nº: BOL0305/2021). The authors would like to thank CNPq for the financial support (Grant number 408135/2021-2) and the State University of Feira de Santana (FINAPESQ/034-2021).

REFERENCES

[1] A. K. Pour, "Experimental and numerical evaluation of steel fibres RC patterns influence on the seismic behaviour of the exterior concrete beam-column connections," *Eng. Struct.*, vol. 263, pp. 114358, 2022, http://doi.org/10.1016/j.engstruct.2022.114358.

[2] Concrete Society, *Concrete Industrial Ground Floors: a Guide To Design and Construction* (Report of a Concrete Society 34). Camberley, 2018.

[3] A. R. Barros, P. C. C. Gomes, and A. S. R. Barboza, "Flexão de vigas de concreto autoadensável reforçado com fibras de aço," *Rev. Assoc. Port. Anal. Exp. Tensoes*, vol. 19, pp. 133–143, 2011.

[4] J. A. Carneiro, "*Uso de agregado reciclado e fibras de aço em concreto simples e concreto armado sob flexão*," M.S. thesis, Depto. Tecnol., Univ. Est. Feira de Santana, Feira de Santana, 2011.

[5] P. D. C. P. Vítor, A. C. Santos, and L. M. Trautwein, "Resistência ao cisalhamento em vigas de concreto armado sem armadura transversal reforçadas com fibras de aço," *Ambient. Constr.*, vol. 18, no. 3, pp. 255–270, 2017, http://doi.org/10.1590/s1678-86212018000300280.

[6] J. A. O. Barros, "*Comportamento de betão reforçado com fibras: análise experimental e simulação numérica*," Ph.D. dissertation, Fac. Eng., Univ. Porto, Porto, 1995.

[7] A. J. B. Viliet, *Bond of Deformed Reinforcing Steel Bars Embedded in Steel Fiber Reinforced Concrete – State-of-the-Art Report.* Delft: Delft Cluster, 2001, pp. 1-66.

[8] W. M. Pereira Jr., D. L. Araújo, and J. J. C. Pituba, "Análise numérica de vigas de concreto com fibras de aço utilizando mecânica do dano," *Rev. IBRACON Estrut. Mater.*, vol. 9, pp. 153–191, 2016.

[9] D. Redaelli, A. Spasojevic, and A. Muttoni, "Experimental and numerical study on the use of high-strength and ultra-high performance fiber reinforced concrete in columns," in *ACI-fib Int. Wksp.*, 2014.

[10] J. Barros et al., "Blind competition on the numerical simulation of steel-fiber-reinforced concrete beams failing in shear," *Struct. Concr.*, vol. 22, no. 2, pp. 939–967, 2021.

[11] J. Barros et al., "Blind competition on the numerical simulation of continuous shallow steel-fiber reinforced concrete beams failing in bending," *Struct. Concr.*, vol. 24, no. 3, pp. 1–31, 2023, http://doi.org/10.1002/suco.202200754.

[12] D. L. Araújo, C. R. Siqueira Fo., and F. A. Lobo, "Computational modeling of plain and steel fiber-reinforced concrete beams without transverse reinforcement," *Rev. IBRACON Estrut. Mater.*, vol. 16, no. 3, e16311, 2023, http://doi.org/10.1590/s1983-41952023000300011.

[13] B. F. Grossi, "*Uma contribuição para a modelagem numérica do concreto com fibras de aço*," Ph.D. dissertation, Depto. Eng. Estrut., Esc. Eng., Univ. Fed. Minas Gerais, Belo Horizonte, 2006.

[14] C. L. Borderie, "*Phénomènes unilatéraux dans un matériau endommageable: modélisation et application à l'analyse de structures en béton*," Ph.D. dissertation, Univ. Paris, Paris, 1991.

[15] P. Grassl, K. Lundgren, and K. Gylltoft, "Concrete in compression: a plasticity theory with a novel hardening law," *Int. J. Solids Struct.*, vol. 39, no. 20, pp. 7021, 2002, http://doi.org/10.1016/S0020-7683(02)00408-0.

[16] V. K. Papanikolaou and A. J. Kappos, "Confinement-sensitive plasticity constitutive model for concrete in triaxial compression," *Int. J. Solids Struct.*, vol. 44, no. 21, pp. 5205, 2007, http://doi.org/10.1016/j.ijsolstr.2007.03.022.

[17] A. Dmitriev, Y. Novozhilov, D. Mikhalyuk, and V. Lalin, "Calibration and validation of the menetrey-willam constitutive model for concrete," *Constr. Unique Buildings Struct.*, vol. 88, pp. 8804, 2020.

[18] Z. Unuk and M. Kuhta, "Nonlinear semi-numeric and finite element analysis of three-point bending tests of notched polymer fiber-reinforced concrete prisms," *Appl. Sci.*, vol. 14, no. 4, pp. 1604, 2024. http://doi.org/10.3390/app14041604.

[19] M. Rashidi, S. Kargar, and S. Roshani, "Experimental and numerical investigation of steel fiber concrete fracture energy," *Structures*, vol. 59, pp. 105792, 2024, http://doi.org/10.1016/j.istruc.2023.105792.

[20] Comité Euro-international du Béton, *Model Code 1990 for Structures.* London: CEB, 1993.

[21] Associação Brasileira de Normas Técnicas, *Projeto de Estruturas de Concreto – Procedimento*, ABNT NBR 6118, 2023.

[22] B. Hansen, "Line ruptures regarded as narrow rupture zones. Basic equations based on kinematic considerations," in *Proc. Conf. Earth Pressure Problems, vol. 3*, Brussels, 1958.

[23] E. V. Pereira, "*influência de fibras de aço no comportamento mecânico e nos mecanismos de fissuração de concretos autoadensáveis*," M.S. thesis, Depto. Eng. Civ. Amb., PUC-Rio, Rio de Janeiro. 2017.

[24] M. Pajak and G. Wandzik, "Laboratory tests of concrete beams reinforced with recycled steel fibres and steel bars," *Materials*, vol. 14, no. 22, pp. 6752, 2021, http://doi.org/10.3390/ma14226752.

[25] Y. Bao, "*Prediction of ductile crack formation in uncracked bodies*," Ph.D. dissertation, Dep. Ocean Eng., Shanghai Jiao Tong Univ., Shanghai, 2003.

[26] P. R. L. Lima, R. D. Toledo Fo., and J. A. Melo Fo., "Compressive stress-strain behaviour of cement mortar-composites reinforced with short sisal fibre," *Mater. Res.*, vol. 17, no. 1, pp. 38–46, 2013, http://doi.org/10.1590/S1516-14392013005000181.

[27] M. Xu and K. Wille, "Fracture energy of UHP-FRC under direct tensile loading applied at low strain rates," *Compos., Part B Eng.*, vol. 80, pp. 116–125, 2015, http://doi.org/10.1016/j.compositesb.2015.05.031.

Author contributions: LMS: conceptualization, methodology, numerical analysis, writing; PRLL: conceptualization, writing, supervision; GJBS: conceptualization, methodology, writing, supervision.

Editors: Samir Maghous, Daniel Cardoso.